Journal of Fluids and Structures 73 (2017) 16–36

Contents lists available at ScienceDirect

Journal of Fluids and Structures

journal homepage: www.elsevier.com/locate/jfs

The role of Reynolds number in the fluid-elastic instability of tube arrays

A. Ghasemi [a,*], N.K.-R. Kevlahan [b]

[a] Department of Mathematics, Technische Universität München, Boltzmannstrasse 3, 85748 Garching, Germany
[b] Department of Mathematics and Statistics, McMaster University, Hamilton L8S 4K1, Canada

ARTICLE INFO

Article history:
Received 21 September 2016
Received in revised form 29 March 2017
Accepted 10 May 2017

Keywords:
Tube array
Vortex-induced vibration
Fluid-elastic instability
Turbulence
Reynolds number
Penalization

ABSTRACT

The onset of fluid-elastic instability in tube arrays is thought to depend primarily on the mean flow velocity, the Scruton number and the natural frequencies of the tubes. However, evidence from experiments suggests that the Reynolds number is also an important parameter, although the available data are insufficient to understand or quantify this effect. We use high resolution direct numerical simulations to solve the penalized two-dimensional Navier–Stokes equations in order to accurately model turbulent flow through tube arrays with a pitch to diameter ratio $P/D = 1.5$. To investigate the Reynolds number effect we perform simulations that independently vary the mean flow velocity and the Reynolds number at fixed Scruton number. Parameters are chosen so that the simulations are well outside the lock-in regime of resonant vortex excitation. Increasing Reynolds number and mean flow velocity both have strong de-stabilizing effects for rotated arrays. For in-line arrays the effect is weaker and not monotonic with increasing Reynolds number and mean flow velocity. This study clarifies how the onset of fluid-elastic instability depends on Reynolds number (and hence turbulence intensity) and reduces uncertainties arising from the experimental data, which usually do not account for the effect of Reynolds number. It also demonstrates the usefulness of two-dimensional direct numerical simulations to investigate fluid-elastic instability at turbulent Reynolds numbers.

1. Introduction

Tube arrays consist of parallel tubes (typically with circular cross-sections) in a periodic pattern and are found in heat exchangers, boilers, condensers and steam generators. Hundreds to thousands of tubes are typically used in heat exchangers depending on the application (Païdoussis et al., 2010). Tube arrays in these installations are subjected to cross-flow, interacting with an external fluid stream which is hotter or colder than the internal flow within the tubes. There are other situations similar to cross-flow in tube arrays. For instance, wind engineering applications where several slender and closely spaced flexible structures are exposed to the high speed wind.

The response of the tubes is a *fluid–structure interaction* (FSI) problem since the tubes often move or bend due to the external fluid forces. The fluid flow is modified in turn by the tube motion. This is therefore a strongly nonlinear coupled problem. Fig. 1 shows various tube array configurations for different industrial applications (Chen, 1987); however in this study, we focus on two cases: in-line and rotated square arrays. Table 1 summarizes the non-dimensional parameters that characterize this problem.

* Corresponding author.
E-mail addresses: ali.ghasemi@tum.de (A. Ghasemi), kevlahan@mcmaster.ca (N.K.-R. Kevlahan).

http://dx.doi.org/10.1016/j.jfluidstructs.2017.05.004
0889-9746/

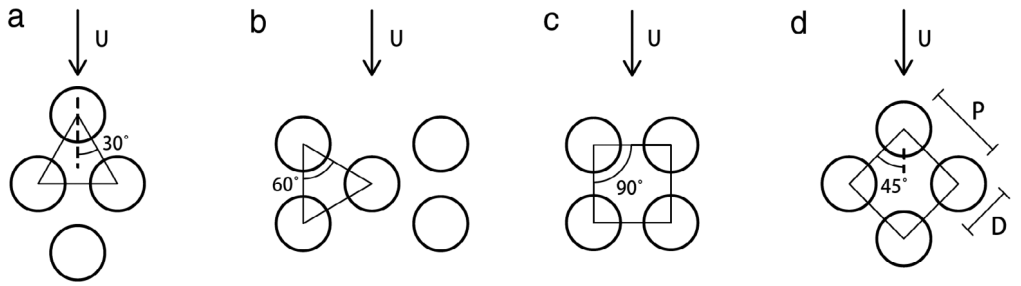

Fig. 1. Basic cross-sectional patterns for tube layout in heat exchangers (Païdoussis et al., 2010). The arrow indicates the direction of the cross-flow U. (a) Normal-triangular, (b) rotated-triangular, (c) normal or in-line square, and (d) rotated or staggered square. We consider in-line and rotated square arrays.

Flow-induced periodic movements (oscillations) of the tubes may cause sudden destruction, especially in tightly packed arrays, if the vibration amplitude exceeds a critical threshold. This phenomenon was not properly identified until the 1960s and has led to many failures. MacDonald et al. (1996) reported a long list of tube failures in power plant steam generators. Damage caused by flow-induced vibration is not limited to equipment containing tube arrays. In 1965 three of eight cooling towers arranged in two parallel staggered rows at the Ferrybridge power station in England collapsed suddenly to the synchronization of the wind-induced vibrations with the natural frequency of the structure (Shellard, 1967).

Many attempts have been made by researchers and engineers to better understand this particular FSI problem. Chen (1968) presented a map of Strouhal numbers for tube arrays as a function of geometry and gap spacing and the data have been used widely for industrial designs by engineers. Connors (1970) introduced the self-excitation phenomenon in tube arrays caused by energy transfer from fluid flow to tubes. He proposed a simplified theory, the displacement mechanism, to evaluate tube instability which was later termed *fluid-elastic instability* (FEI). FEI is characterized by an exponential increase in tube vibration amplitude and is distinct from tube vibration due to resonance with shed vortices. Lever and Weaver (1982) developed a theoretical model for FEI in which instability was attributed to the movement of the separation point on the tube surfaces. Price and Païdoussis (1984) proposed a quasi-static model for the flow-induced forces to analyze the instability for the case of one-degree-of-freedom mechanism. Lever and Weaver (1986a,b) proposed a simplified theory of fluid-elastic instability derived by calculating the forces on a single tube moving periodically in a curved channel. Soon after, Chen (1987) introduced a new model in which fluid forces were simply defined as an empirically determined function of the tube position, velocity and acceleration. Based on experimental measurements Blevins (1984, 2001) proposed a guideline for heat-exchanger design by plotting the critical flow velocity as a function of the mass-damping ratio of tubes. However, he did not explicitly include other parameters such as geometry or gap spacing.

Most importantly, none of these experimental and heuristic theoretical models of FEI account explicitly for the influence of turbulence intensity or Reynolds number. Indeed, even the qualitative effect of turbulence, either stabilizing or de-stabilizing, is unclear in the literature. Nevertheless, the Reynolds number for flow through tube arrays is large enough that the flow is turbulent, $10^3 \leq Re \leq 10^6$ depending on the type of cross-flow fluid (steam, air or water).

Tube excitations are attributed to four distinct mechanisms: *vortex-induced vibrations (VIV)*, *turbulence buffeting*, *acoustic excitation* and *fluid-elastic instability*. In this study, our main focus is the role of turbulence in the FEI mechanism, which is usually the most dangerous form of fluid-induced motion for tube arrays.

Analysis of the cross-flow in tube arrays using analytical or numerical/computational approaches is complicated for two main reasons. First, the geometry of the tube array changes due to the excitations caused by acting fluid forces. Secondly, the flow has a complex coherent vortex shedding structure and becomes turbulent at moderate Reynolds numbers due to the interaction of the fluid with (moving) tubes. The effect of turbulence, as measured by the Reynolds number, on FEI of tube arrays is our main concern in this study. The available data on the effect of turbulence intensity and Reynolds number is conflicting. Indeed, increasing the Reynolds number might be predicted to have either a stabilizing effect (because of increased turbulent damping or a de-stabilizing effect (because of increased fluid forces or a wider range of vortex shedding frequencies). The effect of Reynolds number and turbulence intensity could also depend on the geometry of the array (e.g. in-line or rotated).

Knowing that the turbulence level depends on Reynolds number, Franklin and Soper (1977) claimed that turbulence is *destabilizing*, i.e. it decreases the critical velocity for the onset of FEI. On the other hand, experimental data of Southworth and Zdravkovich (1975) suggest that turbulence has a *stabilizing* effect for the in-line case. Experiments investigating the effect of turbulence are difficult because, for a fixed flow velocity, Reynolds number is a function of kinematic viscosity which makes it difficult to evaluate the effect of Reynolds number and cross-flow velocity separately. In experiments changing viscosity is not easy since it is a basic fluid property and in most cases is only weakly dependent on experimentally controlled variables (e.g. temperature, pressure). Nevertheless, Mewes and Stockmeier (1991) were able to adjust the viscosity in a special fluid mixture and found that *lowering* the viscosity (i.e. increasing the Reynolds number) eliminated FEI in a normal triangular array, again suggesting that turbulence is a stabilizing effect.

In order to clarify the effect of turbulence we use two-dimensional pseudo-spectral direct numerical simulations (DNS) to perform numerical experiments which are very difficult to perform physically. The experiments separate the effects of

Table 1
Key non-dimensional parameters for tube arrays subjected to cross-flow (Blevins, 2001; Nakamura et al., 2013). U is the cross-flow velocity (we use the gap velocity U_g defined in Section 3.3), f_N is the natural frequency of the tubes, D is the diameter of the tubes, ν is the kinematic viscosity, f_S is the vortex shedding frequency, m is the mass per unit length of the tubes, $\delta \approx 2\pi\zeta$ is the logarithmic decrement of tube response (where ζ is the damping ratio of the tubes), ρ is the density of the fluid, and u' are turbulent velocity fluctuations.

Non-dimensional parameter	Definition	Physical meaning
Reduced velocity (U_r)	$\frac{U}{f_N D}$	Normalized cross-flow velocity
Dimensionless amplitude	$\frac{A_y}{D}$	Vibration amplitude/tube diameter
Reynolds number (Re)	$\frac{UD}{\nu}$	Inertia force/viscous force
Strouhal number (St)	$\frac{f_S D}{U}$	Normalized vortex shedding frequency
Scruton number (Sc)	$\frac{2m\delta}{\rho D^2}$	Mass ratio × damping ratio
Turbulence intensity (TI)	$\frac{\langle u' \rangle}{U}$	RMS of turbulence fluctuations/mean flow velocity

reduced velocity and Reynolds number (and hence turbulence intensity). We assume doubly periodic boundary conditions with four tubes in each periodic unit cell. The accuracy of two-dimensional simulations for predicting the onset of FEI for in-line arrays was confirmed in previous work (Kevlahan, 2011; Shinde, 2014) and is explained and validated in detail in Section 4.3. The periodicity assumption is justified by the periodic geometry of industrial tube arrays over many rows, and a 2×2 tube arrangement in the periodic unit cell is the smallest that allows for both in-phase and out-of-phase motions of adjacent tubes (which are the dominant instability modes).

In the following section we review the experimental results and theory of flow-induced vibration phenomenon (Section 2). Then in Section 4 we present the mathematical model and the numerical method. We finally present the simulation results and discuss the results in Sections 5 and 6. The main conclusions of the study are summarized in Section 7.

2. Flow-induced vibration (FIV) in tube arrays

Flexibly mounted tube arrays, subjected to cross-flow, begin to vibrate due to the energy gained from the fluctuating forces (drag and lift) exerted by the fluid. Flow past a fixed tube array has a complicated structure; however, interaction of the moving tubes with the fluid and adjacent tubes increases the flow complexity due to the interaction of the moving wakes from adjacent rows and columns of tubes.

In this section we briefly review the various types of vibrational responses (excitation mechanisms) of tubes in cross-flow caused by lock-in, fluid-elastic instability and turbulence buffeting (excluding acoustic excitation) using the classification introduced by Chen (1987) (Fig. 3). In particular, we consider the effects of parameters such as flow velocity, turbulence level, Scruton number, natural frequency and geometry of the array on excitations and instability.

2.1. Vortex-induced vibration (VIV)

When a fluid passes a structure sufficiently rapidly (e.g. $Re > 60$), it generates vortices in the wake region behind the body. This phenomenon (also known as Kármán vortex shedding) imposes a periodic surface pressure on the body causing flexible structures to oscillate. The vortex street formed behind the structure and parallel to the flow direction, regardless of the geometry of the structure, are usually similar. The vortex shedding frequency is characterized by a non-dimensional parameter called the Strouhal number St,

$$St = \frac{f_S D}{U}, \tag{1}$$

where f_S is the vortex shedding frequency, U is the cross-flow velocity (usually the mean or up-stream velocity U_∞ or sometimes the mean velocity in the gap between tubes U_g), and D is the characteristic length scale of the structure. The Strouhal number increases with increasing packing density (pitch to diameter ratio) of the array from about 0.2 (for an isolated tube) to about 0.5 for an in-line array (Fitzhugh, 1973) based on gap flow velocity U_g (or $St = 6.0$ based on upstream velocity U_∞).

The Strouhal number is important because tube motion is excited if the vortex shedding frequency is close to one of the natural mechanical frequencies of the tube 3. Since the rate of energy input can exceed the rate of energy damping in the array, high amplitude vibrations (resonance) may occur. This phenomenon is known as the *lock-in* mechanism and must be avoided in tube arrays due to the possibility of destroying the tube array. American Society of Mechanical Engineers (ASME) design standards (ASME, 1995) propose an empirical guideline for the range of frequency ratios to be avoided,

$$|f_N - f_S| \geq 0.3 f_N, \tag{2}$$

or equivalently, in terms of reduced velocity U_r and Strouhal number St we require that

$$U_r \leq 0.7/St \quad \text{and} \quad U_r \geq 1.3/St. \tag{3}$$

For the in-line arrays considered here we should ensure that the critical velocity $U_{cr} \geq 3.7$ to ensure FEI is well-separated from lock-in. Similarly, we should ensure $U_{cr} \geq 2.6$ to avoid lock-in for the rotated arrays.

Vortex induced vibration is an important phenomenon for three reasons. First, the vortex shedding frequency bandwidth is not always narrow, particularly in turbulent flows, and excitation may occur if the vortex shedding frequency band overlaps the natural frequency of the tubes. Secondly, lock-in may cause transitory oscillations in the tubes if the flow velocity is gradually increased from zero to its operating value if the operating value exceeds (3). Finally, although synchronization mostly occurs in transverse oscillations (caused by lift force) in high-density fluid flows can induce stream-wise vibrations at a frequency approximately twice the vortex shedding frequency ($2f_S$) (Chen, 1978; Nakamura et al., 2013). Therefore, in the present work we have been careful to choose parameters such that the lock-in region is well-separated from the region of fluid elastic instability (see Section 2.2).

2.2. Fluid-elastic (self-excited) instability (FEI)

Roberts (1966) was probably the first to observe that a single row of tubes responded to cross-flow by high amplitude transverse vibrations well *outside* the lock-in region. He proposed that the phase lag between periodic fluid forces and periodic tubes displacement (response) is the cause of such behavior. Four years later Connors (1970) used linear stability analysis (assuming induced flow forces varies due to the interaction of adjacent tubes) to suggest a similar displacement-induced vibration mechanism. Connors' quasi-static model predicted that the critical velocity for FEI scales like the square root of Scruton number. FEI is the main cause of short term damage in heat exchangers (Païdoussis et al., 2010).

More precisely, FEI is usually understood as an "negative damping" of tube oscillations where a phase lag between the fluctuating tube motion and fluid forces produces an effective negative damping in the simple harmonic oscillator model for tube vibration. The response of an individual tube is modeled as a simple harmonic oscillator, where the fluid forcing due to vortex induced vibration or turbulence reduces the effective damping ratio. For sufficiently large cross-flow velocities the phase lag between the periodic motion of the tubes and the periodic fluid forces generates a net negative damping ratio that causes the amplitude of tube oscillation to increase exponentially with increasing flow velocity. Note, however, that the negative damping explanation was not verified in a numerical study that carefully separates potential flow and vortical effects (Kevlahan, 2011). In particular, the negative damping theory was found to significantly overestimate the onset of FEI. The negative damping explanation, although intuitively reasonable and leading to qualitatively accurate results, is incomplete.

Evidence from experiments suggests that the critical flow velocity (onset of FEI) scales approximately with Scruton number (Table 1) like

$$\frac{U_{cr}}{f_N D} = C Sc^{\alpha}. \tag{4}$$

Experimentally derived constants a and b are given in Table 2. The given critical velocity U_{cr} is a conservative lower bound for the onset of instability (Chen, 1987) and not a precise characterization of the onset of instability. Note that the effects of turbulence intensity and Reynolds number are not accounted for independently of cross-flow velocity. A widely used experimental dataset for prediction of FEI is the empirical data published by Blevins (1984), which simply shows the stable and unstable regions based on a scaling like $CSc^{1/2}$ (as found by Connors (1970)) with constant $C = 1.7$ picked so the stability bound is below 90% of the available experimental data for $Sc > 1.4$ (Fig. 2). We will mostly refer to these data, since both the lower bound (conservative) and the mean value of the critical velocity are illustrated. The square root scaling appears to be valid except at very low Scruton numbers, although the semi-empirical model of Lever and Weaver (1986a,b) (discussed below) predicts a linear scaling for large Scruton numbers.

Combining this conservative FEI criterion $U_{cr} \geq 1.7Sc^{1/2}$ with (3) suggests that to clearly separate lock-in from FEI we require

$$Sc \geq 0.59/St^2. \tag{5}$$

Therefore, since $St \approx 0.35$ for the in-line arrays we consider and $St \approx 0.5$ for the rotated arrays we require $Sc \geq 4.8$ or $Sc \geq 2.3$ respectively. At smaller Scruton numbers the effects of lock-in and FEI are combined. In addition, the theory of Lever and Weaver (1986b) predicts multiple regions of FEI stability at small Scruton numbers (see Fig. 2).

A simple semi-empirical model of FEI based on modeling the flow as a single vibrating tube in a curved channel was developed by Lever and Weaver (1986a,b). This model gives a linear, rather than square root, scaling $U_c \propto Sc$ for $Sc \gg 1$, but predicts multiple stability regions for fixed small Scruton number below an array-dependent threshold (see Fig. 2). The linear scaling for large Scruton numbers appears to be inconsistent with the experimental data, but the multiple stability regions is consistent with the spread of data points at small Scruton number. Again, this model does not include turbulence effects and is based on a negative damping mechanism for FEI due to a phase lag between fluid forces and tube motion.

Table 2
Lower bounds (Chen, 1987) on critical velocity for in-line and rotated square tube arrays: the critical velocity is assumed to scale like CSc^{α}. P/D is the pitch to diameter ratio characterizing the spacing of the array. Note that the relevant structural parameters are measured in vacuum.

		C	α
In-line square	$0.06 < Sc < 1.40$	1.48	0.15
	$1.40 < Sc < 600$	1.66	0.50
Rotated square	$0.20 < Sc < 600$	$2.50(P/D - 0.5)$	0.50

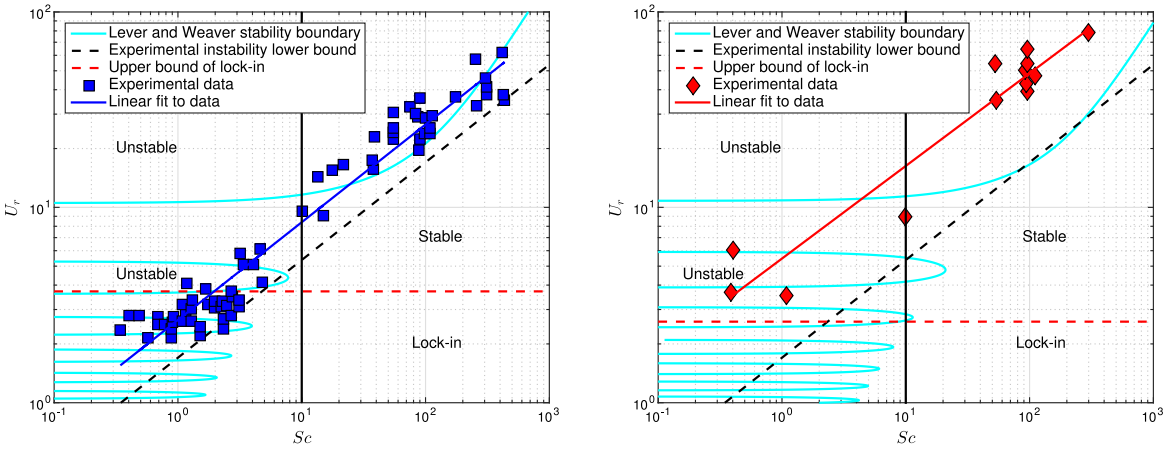

(a) In-line arrays. (b) Rotated arrays.

Fig. 2. Onset of fluid-elastic instability as a function of Scruton number for in-line and rotated arrays with $P/D = 1.5$. The experimental data is for a variety of experiments with different arrays (extracted from Figures 5–6 in (Blevins, 2001)) and the stability curves are calculated from the semi-empirical theory of Lever and Weaver (1986b). Note that lock-in is well-separated from the region of FEI for sufficiently large Scruton number. The vertical line shows the fixed $Sc = 10$ value used for the Reynolds number dependence simulations.

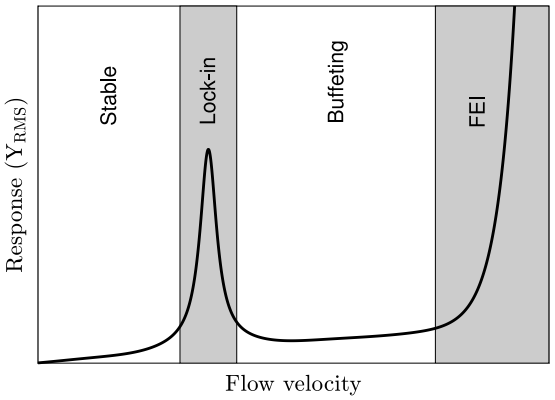

Fig. 3. Different types of response in a tube array subject to cross-flow: lock-in, turbulence buffeting and fluid-elastic instability. *Source:* (modified from Chen (1987))

2.3. Turbulence (random) buffeting

At higher cross-flow velocities and Reynolds numbers turbulence fluctuations begin to buffet the tubes. In turbulent flow random pressure distributions on the surfaces of the tubes induces low amplitude vibrations in which the excitation level depends on turbulence intensity (TI) and the random behavior of the flow due to the upstream flow turbulence or the turbulence generated in the tube array itself. In general, the turbulence level increases with increasing Reynolds number (Chen, 1987). Fig. 3 shows how the vibration amplitude varies with flow velocity (and with Reynolds number). The turbulence induced vibration amplitude is not usually high enough to constitute a problem. However, random excitation may induce or modify lock-in or FEI.

Some experiments have demonstrated that the increases in upstream turbulence intensity can either stabilize or destabilize self-excited vibrations by increasing or decreasing the critical velocity. This is strong evidence that the Reynolds number is an important parameter which needs to be accounted for independently of other parameters, such as reduced velocity and mass-damping ratio, and motivates our numerical study. On the other hand, other experiments have shown little or no effect of turbulence on instability of tube arrays. Chen and Jendrzejczyk (1981) performed water-tunnel tests that partially resolved this problem; depending on the turbulence characteristics of the flow, both stabilizing and destabilizing effects exists. This statement was verified later by Soper (1982).

The best attempt to study the effect of Reynolds number itself, independent of other flow properties, on fluid-elastic instability was performed by Mewes and Stockmeier (1991). They made measurements on flow induced instability using a fluid mixture whose viscosity could be varied such that $0.7 \leq \nu/\nu_{water} \leq 87.3$. They were able to eliminate FEI in a normal triangular array by decreasing ν/ν_{water} from 2.52 to 0.7 (i.e. increasing the Reynolds number).

The role of turbulence in FIV is entangled with both cross-flow velocity (the vertical axis in Fig. 2) and Scruton number (the horizontal axis in Fig. 2). If the fluid is not changed, the Reynolds number increases proportional to cross-flow velocity. Low Scruton numbers are associated with high Reynolds numbers (e.g. $Re = O(10^6)$ for water at $Sc = O(10^{-1})$), while high Scruton numbers are associated with low Reynolds numbers (e.g. $Re = O(10^4)$ at $Sc = 10^2$ for water vapor).

In principle, we expect that increasing Reynolds number should affect stability in three main ways. First, increased turbulence could increase the effective fluid damping due to increased turbulence damping, thus stabilizing the tubes. Secondly, the vortex shedding frequency spectrum could broaden, with multiple shedding frequencies, as the flow becomes more turbulent (see Fig. 17). Therefore, there is a possibility that the presence of multiple shedding frequencies increases the chance of exciting an unstable oscillation mode. Thirdly, turbulence intensity could increase, which might lead to more intense vorticity and hence higher fluctuating fluid forces that could trigger an instability.

Although turbulence buffeting has been a well-known factor in tube excitations for decades, the question of precisely how turbulence affects the stability of tube arrays, particularly the FEI instability, remains open and is the main subject of the present investigation.

3. Mathematical model

In the previous section we reviewed the three main classes of flow-induced vibration of tube arrays (lock-in, turbulence buffeting and FEI) and the main empirical models for FEI (based on negative damping). The role of turbulence is rarely examined explicitly, and when it is found to sometimes destabilize and sometimes stabilize the tube response.

In this section we describe how we efficiently and accurately model the problem in order to better understand the role of Reynolds number and turbulence in the onset of FEI.

We begin with a mathematical formulation for modeling fluid flow past tube arrays, and then describe the numerical methods used for solving those mathematical models. Finally, the dynamical model for the interaction of tubes with the fluid or other tubes is presented. Since computational cost and efficiency of the method is of primary importance, some notable features of the pseudo-spectral numerical are described.

Because accurately computing turbulence is essential, we use a direct numerical simulation (DNS) approach to resolve all active length scales of the flow without subgrid scale turbulence models.

3.1. Fluid equations

In this section we describe concisely the model used for this particular fluid–structure interaction problem, originally developed by Kevlahan and Ghidaglia (2001). As mentioned in the introduction, we use a two-dimensional approximation to the fluid flow and tube response with doubly periodic boundary conditions.

The Navier–Stokes equations for a fixed mean flow $\mathbf{U}_\infty$ are

$$\frac{\partial \mathbf{u}}{\partial t} + (\mathbf{u} + \mathbf{U}_\infty) \cdot \nabla \mathbf{u} + \frac{1}{\rho} \nabla P = \nu \Delta \mathbf{u}, \tag{6}$$

where $\mathbf{u}$ is fluid velocity, P is the absolute pressure, ρ the fluid density (assumed constant) and ν the viscosity. The mass continuity equation (conservation of mass) for incompressible flow is

$$\nabla \cdot \mathbf{u} = 0. \tag{7}$$

Eqs. (6) and (7) model fluid flow without solid boundaries. Explicitly imposing no-slip boundary conditions on moving tubes is numerically very difficult, especially in a pseudo-spectral method. Therefore, we implicitly impose a Dirichlet no-slip boundary condition using a Brinkman volume penalization technique (Kevlahan and Ghidaglia, 2001). In other words, instead of modifying the boundary conditions we modify the equations in such a way that the solution of the new equations on the original periodic domain approximates the solution of the Navier–Stokes equations with moving solid tubes. Thus, instead of $\mathbf{u}$ in the Eqs. (6), (7), we solve for the penalized velocity $\mathbf{u}_\eta$ as

$$\frac{\partial \mathbf{u}_\eta}{\partial t} + \left(\mathbf{u}_\eta + \mathbf{U}_\infty\right) \cdot \nabla \mathbf{u}_\eta + \frac{1}{\rho} \nabla P = \nu \Delta \mathbf{u}_\eta - \frac{1}{\eta} \chi(\mathbf{x}, t)(\mathbf{u}_\eta + \mathbf{U}_\infty - \mathbf{U}_{o,i}), \tag{8}$$

$$\nabla \cdot \mathbf{u}_\eta = 0, \tag{9}$$

where $\mathbf{U}_{o,i}$ is the velocity of the ith tube and η is the penalization control parameter (permeability constant) which is very small ($0 < \eta \ll 1$). The characteristic function $\chi(\mathbf{x}, t)$ defines the solid regions to be penalized,

$$\chi(\mathbf{x}, t) = \begin{cases} 1 & \text{if } \mathbf{x} \in \Omega_i \ \forall i, \\ 0 & \text{otherwise,} \end{cases} \tag{10}$$

in which Ω_i denotes ith solid zone (tube). Carbou and Fabrie proved that the solution of Eqs. (8), (9) converges to the solution of incompressible Navier–Stokes equations (6), (7) and the upper bound on global error of the penalized Navier–Stokes is (Carbou et al., 2003)

$$\|\mathbf{u} - \mathbf{u}_\eta\|_2 \leq C\eta^{\frac{1}{2}} \text{ in } L^2(\Omega_f), \tag{11}$$

where Ω_f is the fluid part of the domain. Therefore, by choosing the control parameter η sufficiently small we can enforce the no-slip boundary condition on the (moving) tubes to the desired tolerance.

The Brinkman volume penalization method imposes the no-slip condition automatically since the solution for $\mathbf{u}_\eta$ is always approximately equal to the tube velocity ($\mathbf{U}_{o,i}$) on the edge of fluid–solid surface. The boundary conditions on Eqs. (8), (9) are summarized below:

$$\begin{cases} \mathbf{u} + \mathbf{U}_\infty = \mathbf{U}_{o,i} \text{ on } \Omega_i \ \forall i, \\ \mathbf{u} \text{ is } Q\text{-periodic}, \quad Q =]0, L_1[\ \times \ ]0, L_2[. \end{cases} \tag{12}$$

3.2. Tube equations

The fluid forces $\mathbf{F}_i$ acting on the surface of the tubes are calculated simply by integrating the penalization term over the cross-sectional area of the tube (Angot et al., 1999),

$$\mathbf{F}_i = \frac{1}{\eta} \oint_{\Omega_i} (\mathbf{u} + \mathbf{U}_\infty - \mathbf{U}_{o,i}) d\mathbf{x}. \tag{13}$$

It has been proved analytically that the error in the calculated forces are also $O(\eta^{\frac{1}{2}})$ (Angot et al., 1999) and it was shown by Kevlahan and Wadsley (2005) that the actual error for computed drag force is about 1% if the penalization parameter $\eta = 10^{-4}$ (for appropriate non-dimensional variables).

Considering the fluid forces to be the only external forces acting on the tubes, the response of tubes is modeled by the damped simple harmonic oscillation equation and in standard form written as

$$\frac{d^2\mathbf{X}_{o,i}}{dt^2} + 2\zeta\omega_N \frac{d\mathbf{X}_{o,i}}{dt} + \omega_N^2 \mathbf{X}_{o,i} = \frac{\mathbf{F}_i}{m}, \tag{14}$$

where $\mathbf{X}_{o,i}$ are the tube positions, m is mass per unit length of tubes, $\mathbf{F}_i$ is the external forcing due to the fluid motion, the important parameters $\zeta = c/(2\sqrt{km})$ is the damping ratio, and $\omega_N = 2\pi f_N = \sqrt{k/m}$ (the undamped angular frequency) in which c is damping coefficient and k is the spring constant. Note that c and k are values based on vacuum or uncoupled fluid-tube measurements and there is additional damping due to the surrounding fluid (included in $\mathbf{F}_i$). We assume that all tubes are mechanically identical. All tubes are free to vibrate in both the streamwise and transverse directions.

We use Eq. (13) to compute the fluid forces $\mathbf{F}_i$ in Eq. (14) which results in a simple ordinary differential equation (ODE) problem for the forced simple harmonic oscillator.

In some cases two or more tubes can clash or hit each other. This phenomenon mostly occurs in tightly packed arrays and when the tubes are highly unstable or have anti-phase vibrations. Although we can easily observe the collision between tubes during the simulation, interpret it as an unstable case and stop the simulation, we have seen stable situations in which some transient oscillations caused collisions. It is therefore necessary to consider the situation when tubes can collide.

Ignoring change of total momentum at the moment of collision (i.e. assume that $\int_t^{t+\delta t} \mathbf{F_i} dt = 0$), we can write conservation of momentum for the interaction of two tubes (i, j) as

$$\begin{cases} \mathbf{U}_{n,i}^k = \frac{1}{2}(1-\alpha)\mathbf{U}_{n,i}^{k-1} + \frac{1}{2}(1+\alpha)\mathbf{U}_{n,j}^{k-1}, \\ \mathbf{U}_{n,j}^k = \frac{1}{2}(1-\alpha)\mathbf{U}_{n,j}^{k-1} + \frac{1}{2}(1+\alpha)\mathbf{U}_{n,i}^{k-1}, \end{cases} \tag{15}$$

and

$$\begin{cases} \mathbf{U}_{t,i}^k = \mathbf{U}_{t,i}^{k-1}, \\ \mathbf{U}_{t,j}^k = \mathbf{U}_{t,j}^{k-1}, \end{cases} \tag{16}$$

where indices $k-1$, k denote time steps before and after collision, respectively. α is the restitution coefficient and equals zero for totally elastic and one for completely inelastic impacts. For two steel bodies colliding with small relative velocities, α is close to one (Meriam and Kraige, 2013). Notation "n" stands for velocity components in direction of the impact and "t" for directions tangent to contact line between tubes. Note that the tubes might impact in any direction since the domain is periodic.

3.3. Mean and gap velocity and the definition of Reynolds number

There are two different definitions for the average cross-flow velocity in tube arrays. First, is the mean upstream flow velocity referred as U_∞. The second and most commonly used definition is the mean velocity in the minimum gap between the (fixed) tubes, referred to as U_g. For in-line square arrays, the relation between these two definitions is

$$U_g = \frac{P}{P-D} U_\infty. \tag{17}$$

For square rotated (staggered) arrays, depending on pitch-to-diameter ratio, the gap velocity is

$$\begin{cases} U_g = \dfrac{\sqrt{2}P/D}{2(P/D-1)} U_\infty, \text{ if } 1 < \dfrac{P}{D} \leq \dfrac{1}{2-\sqrt{2}}, \\ U_g = \dfrac{\sqrt{2}P/D}{\sqrt{2}P/D-1} U_\infty, \text{ if } \dfrac{P}{D} > \dfrac{1}{2-\sqrt{2}}. \end{cases} \tag{18}$$

Consequently there are two different Reynolds numbers corresponding to two different definitions of characteristic flow velocities, and the Reynolds number based on gap velocity is higher. When $P/D = 1.5$, as in our case, $Re_g = 3Re_\infty$ for the in-line square array and $Re_g = 3/\sqrt{2}Re_\infty \approx 2.12Re_\infty$ for the rotated array. In the following sections we will mostly use U_g to define Strouhal number, reduced velocity and Reynolds number, although previous experimental results have been expressed based on both definitions.

In the following section we briefly describe the pseudo-spectral numerical method used to solve the model equations derived in this section. This numerical method is chosen for its accuracy and efficiency at high Reynolds numbers.

3.4. Determination of critical flow velocity in tube arrays

Since our goal is to determine how Reynolds number influences FEI, it is important to define an accurate and robust criterion for the onset of instability. As discussed in Section 2.2, the critical flow velocity U_{cr} for FEI is defined as the velocity at which the tube oscillation amplitude starts to increase exponentially. Chen (1987) defines U_{cr} as follows: let the position of a cylinder be

$$X(t) = A\exp((\lambda + i\omega)t). \tag{19}$$

The vibration is damped (stable) if λ is negative. In contrast, the tube motion amplitude increases with time (unstable state) if λ is positive. Therefore, U_{cr} is defined as the velocity at which λ changes sign. In practice, U_{cr} is determined by the point at which the RMS tube vibration begins to increase exponentially (see Fig. 3).

In a similar manner, we define U_{cr} in three steps. First, we plot the tube response (Y_{RMS}) with respect to upstream flow velocity. Secondly, similar to Chung and Chu (2006), we check that the FEI region is well-separated from the turbulent buffeting region. Finally, as shown in Fig. 4 and in Soper (1983), we define U_{cr} using the intersection of the best fitted line to the FEI part of the curve with flow velocity axis. The advantage of this definition is that U_{cr} is specified independent of buffeting mechanism. The validity of this procedure for defining U_{cr} is confirmed below in Section 4.3.

Note that in this study the total response of the tube array (RMS values in the transverse flow direction) is calculated using the average of RMS values for all tubes. However, for highly unstable cases the total response may be averaged over only some of the tubes in the array. This is due to the complex dynamic of a tightly packed array in which strong oscillations of a tube may suppress motion of its neighbors due to clashing.

4. Numerical method

4.1. Discretization

Since the problem is naturally doubly periodic, we solve the model equations presented in Section 3 using a standard Fourier pseudo-spectral scheme similar to that described by Kevlahan (2011). This method is accurate and efficient on periodic domains and has been found to work well with the Brinkman penalization approximation. The Fourier transforms are performed using the FFTW 3.3.4 library and the code is parallelized using `mpi`. Adaptive time stepping is done using a third-order four stage strong-stability-preserving Runge–Kutta method (Spiteri and Ruuth, 2002). The same Runge–Kutta method is used for the tube equations. The computations were done on a variety of parallel machines using up to 128 cores.

For accurate and stable results it is important to resolve the turbulence dynamics, which means fully resolving the thin vortical boundary layer that develops around the tubes. The thickness of this boundary layer, λ, depends on the tube diameter D and Reynolds number Re_g as

$$\lambda \sim \frac{D}{\sqrt{Re_g}}. \tag{20}$$

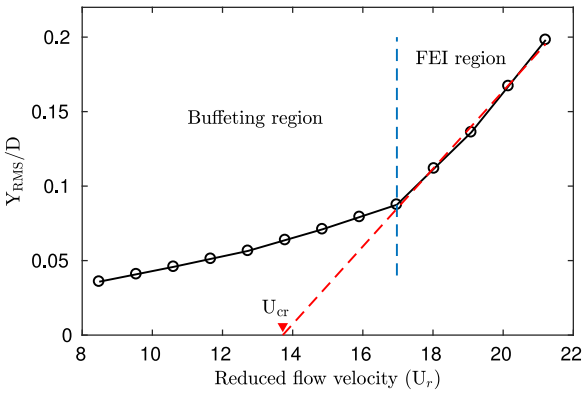

Fig. 4. The critical flow velocity (U_{cr}) is defined by the intersection of the best line fitted to data in the FEI region and the flow velocity axis.

A sufficient number of grid points (N_B) is needed in the pseudo-spectral/penalization method to fully capture the boundary layer. This gives

$$\lambda \geq N_B \Delta x = N_B \frac{L}{N},$$

where Δx is the grid spacing, L is the size of the (square) computational domain and N is the number of collocation points in each direction. Therefore, since the grid points are equally spaced, the minimum number of grid points in each direction of the domain is

$$N \geq N_B N_T \frac{P}{D} \sqrt{Re_g}, \tag{21}$$

where N_T is number of tube rows (or columns) per periodic unit cell ($N_T = 2$ for our simulations). An appropriate level of resolution N_B is determined by grid convergence tests of the relevant quantities (in this case, RMS lift, drag and tube oscillation amplitude).

The grid convergence tests for RMS lift, drag and transverse tube oscillation amplitude presented in Fig. 5 demonstrate that resolving the boundary layer with $N_B = 4$ points is sufficient to give well-converged statistics (results are converged to at least 1%). The number of grid points increases with Reynolds number like $Re_g^{1/2}$ but, because we use a penalization technique, the grid does not need to change in time to track the motion of the tubes.

Since we simulate Reynolds numbers in the range $150 \leq Re_g \leq 2.7 \times 10^4$, the number of grid points N in each direction varies between 128 and 2048, or a total of up to four million grid points. Note that the simulations must be run for very long times, typically $O(10^3)$ non-dimensional tube crossing times, to capture the instabilities and obtain stationary statistics.

4.2. Boundary smoothing

Approximation of a discontinuous function using Fourier series produces localized errors Gibbs oscillations near the discontinuity (Trefethen, 2000). In order to reduce these errors around the penalized region we need to modify the discontinuous region (Eq. (10)) by smoothing the edge of solid–fluid surface. Since the tubes are circular cylinders it is easy to smooth the cylinder edge using a truncated hyperbolic tangent function,

$$\chi(\mathbf{x}, t) = \frac{1}{2}\left(1 - \tanh\left(\frac{r(x,t) - D/2}{W}\right)\right), \tag{22}$$

where r corresponds to the distance from center of cylinder and W is a parameter to control the width of the smoothed band around a cylinder. The solid–fluid boundary is smoothed over three to four grid points. This smoothing has been found to give good results and not significantly modify the fluid forces or boundary layer flow (Kevlahan and Ghidaglia, 2001; Kevlahan and Wadsley, 2005; Kevlahan, 2011).

4.3. Validity of the two-dimensional approximation and definition of U_{cr}

Turbulent flow is naturally three dimensional, and obviously two dimensional simulations neglect non-spanwise components of vorticity and its effect on the fluid forces and resulting tube vibration. Since in static tube arrays non-spanwise vorticity develops at $Re = O(10^2)$ (Kevlahan, 2007), the cases we consider here are all strictly three-dimensional. Nevertheless, the geometry of the tube array means that spanwise correlations are enhanced and spanwise vorticity is dominant. Three-dimensional simulations are extremely costly if they are to resolve a sufficient spanwise length

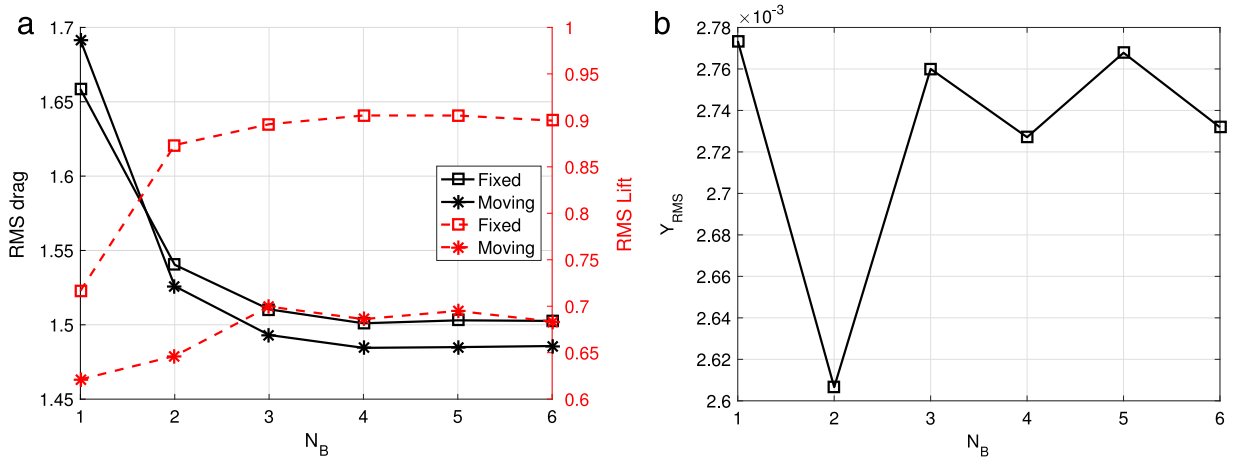

Fig. 5. Grid convergence tests for the numerical scheme as a function of the number of points N_B resolving the boundary layer. The 1×1 rotated tube configuration and $Re_\infty = 200$, $Sc = 2$ is used for the moving cases. (a) RMS drag (left axis, black) and lift (right axis, red) for both the fixed and moving cylinder cases. (b) RMS cylinder oscillation amplitude in the transverse direction. These results show that the force calculations are fully converged for $N_B = 4$ points in the boundary layer. (For interpretation of the references to color in this figure legend, the reader is referred to the web version of this article.)

(typically $O(10)$ tube diameters). Because of this computational cost, even at moderate Reynolds numbers three-dimensional simulations rely on some sort of more or less arbitrary turbulence model, such as unsteady Reynolds averaged Navier–Stokes (URANS) or large eddy simulation (LES). These turbulence models cannot resolve all scales of motion and introduce their own errors, which are particularly significant when it is the effect of the turbulence itself that is the object of study.

It is not clear which compromise (two-dimensional geometry or turbulence models) is best for studying the specific question at hand: the effect of Reynolds number on the critical velocity for the onset of FEI in tube arrays. The key question is whether those properties of the flow that determine the onset of FEI are sufficiently well-captured by two-dimensional DNS.

Sarpkaya (2004)'s review noted that the degree of spanwise correlation is an important factor in VIV in general. However, he considered the existing numerical turbulence models, both RANS and LES, to be inadequate while three-dimensional DNS was limited to moderate Reynolds numbers. In the following we discuss recent numerical simulations that suggest that two-dimensional simulations with a good representation of turbulence can nevertheless accurately estimate the onset of FEI in tube arrays. We also present results from our own simulations confirming this conclusion.

Shinde (2014) simulated URANS turbulent flow through a fixed tube array at $Re_g = 2840$ and observed that the flow is approximately uniform in span-wise direction. In addition, Kevlahan and Wadsley (2005) found that at low Reynolds numbers tube vibration could completely suppress the three-dimensional flow instability, in the sense that for the moving cylinder case the flow is close to two-dimensional. At $Re_g = 6.0 \times 10^4$ for a moving cylinder Shinde (2014) directly compared two- and three-dimensional URANS simulations and found that tube oscillation frequencies were well-predicted by two-dimensional simulations, although the vibration amplitudes in the unstable three-dimensional case were about 30% higher than in two-dimensional case. He also found that the results were highly dependent on the type of URANS model chosen, with some models performing quite poorly.

Most importantly, in a sequence of simulations at Reynolds numbers varying from 1.5×10^4 to 5.1×10^4, Shinde et al. (2015) found that the experimentally measured Reynolds number for the onset of FEI (equivalent to critical velocity) is well predicted by two-dimensional URANS simulations, even though they may under-estimate the tube oscillation amplitude. Indeed, they conclude that two-dimensional simulations are appropriate for developing design standards for heat exchangers that avoid FEI.

On balance, this evidence suggests that two-dimensional DNS is an appropriate choice in the present investigation, since such simulations are able to reach much higher Reynolds numbers and do not require choosing and tuning a turbulence model. DNS resolves all active length scales and temporal frequencies, which is important for accurate FEI calculations. Below we present two separate verifications of the accuracy of our two-dimensional simulations that are relevant for FEI.

As a first partial validation of our two-dimensional simulations we compare calculated Strouhal numbers with experimental measurements. An accurate Strouhal number (i.e. the dominant vortex shedding frequency) is necessary to properly capture the onset of FEI. As shown in Fig. 6, the simulation results for Strouhal numbers in the rotated array are consistent with the experimental data. In addition, for the case of the in-line array, Fitzhugh (1973)'s figure showing the dependence of Strouhal number on array spacing gives $St = 1.02$ for a spacing $P/D = 1.5$ at an unknown Reynolds number. This experimental result is also consistent with the numerical results shown later in Section 6 in Fig. 17: $St = 1.10$ at $Re_\infty = 200$ and $St = 0.98$ at $Re_\infty = 400$. (All Strouhal numbers in this section are based on U_∞.)

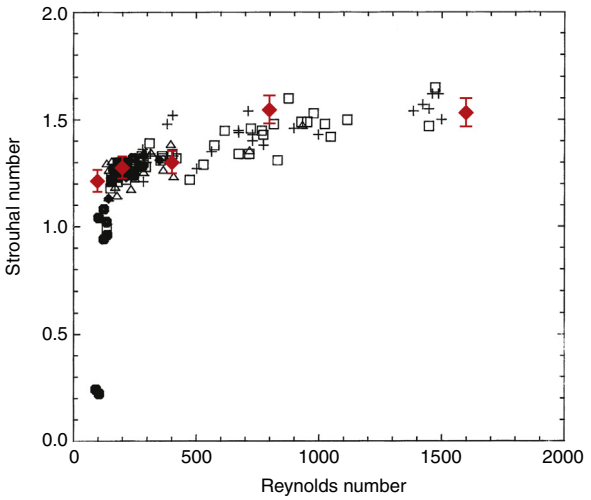

Fig. 6. Plot of Strouhal number versus Reynolds number in rotated square array (modified from (Price et al., 1995)). Black symbols correspond to experimental measurements for different rows in the array and added red diamond signs denote to the simulation results. The Strouhal number and Reynolds numbers are defined using the upstream velocity U_∞.

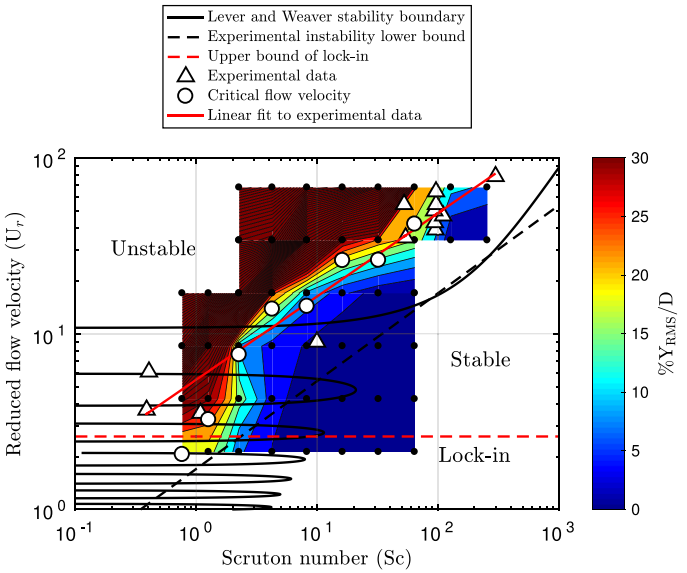

Fig. 7. Dependence of tube vibration amplitude on reduced velocity U_r and Scruton number Sc for the rotated array with $P/D = 1.5$ at Reynolds number $Re_g = 1060$ ($Re_\infty = 500$). The numerical results are compared with experimental results from Figures 5–6 in Blevins (2001) and the theory of Lever and Weaver (1986a,b). The white circles show the critical flow velocities based on the definition presented in Section 3.4.

Since Strouhal number is known to be relatively insensitive to three-dimensional effects in tube arrays, we also verify our calculations directly against experimental data for the onset of FEI in Fig. 7. This is a direct test of the ability of our method to accurately compute the onset of FEI. We plot contours of RMS tube vibration amplitude for the rotated array as a function of reduced velocity U_r and Reynolds number Re_g compared to experimental data and the stability theory shown in Fig. 2(b). The white circles showing the numerical FEI stability threshold confirm that our two-dimensional model and definition of U_{cr} give results for U_{cr} that are qualitatively consistent with experiment. Interestingly, there is some evidence at low $Sc < 4$ of the additional unstable regions corresponding to the unstable "tongues" proposed in the theory of Lever and Weaver (1986a). The stability bound is certainly inconsistent with the simple $Sc^{1/2}$ scaling at these small Scruton numbers.

Fig. 8 shows RMS tube response compared to flow velocity for various Sc numbers, confirming the exponential growth of tube response consistent with the definition of FEI. Similarly, Fig. 9 confirms that in the FEI regime tube oscillation amplitude also grows exponentially in time. The large amplitudes are clearly not due to turbulence buffeting. These results verify that our procedure for identifying the critical velocity does indeed correspond to the usual definition of FEI.

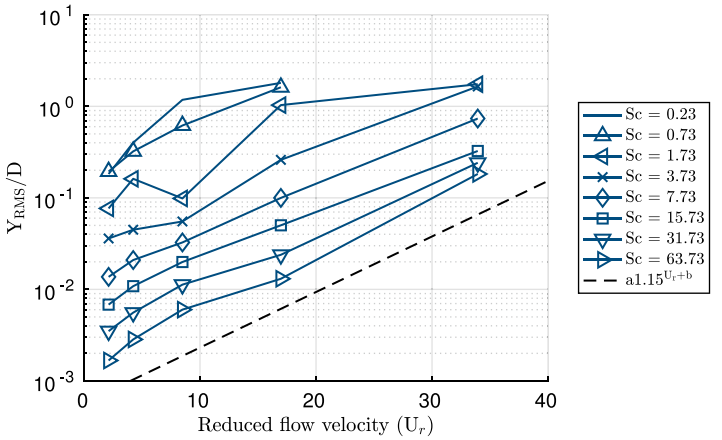

Fig. 8. Semi-logarithmic plot of RMS values versus flow velocity, based on Fig. 7 compared with exponential growth (dashed line).

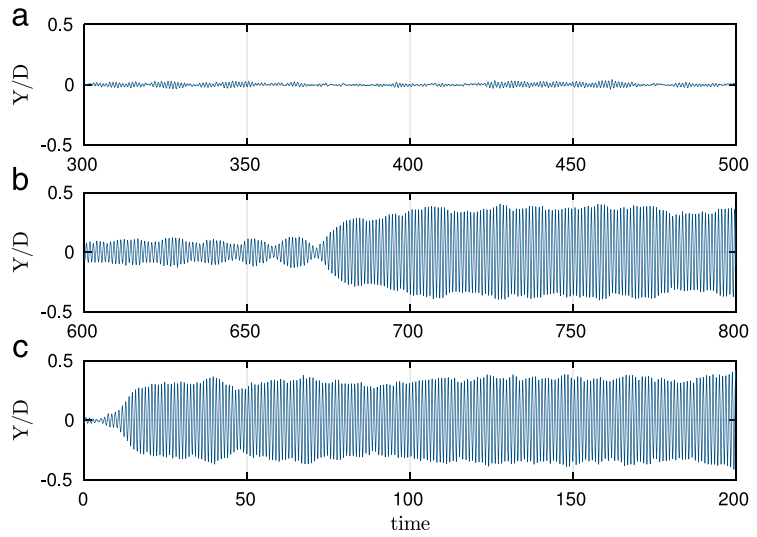

Fig. 9. Response of a tube in an in-line array subjected to flows at $U_{r,\infty}$ equal to (a) 2.4 (stable), (b) 2.8 (close to instability threshold) and (c) 3.2 (unstable).

The good qualitative results for U_{cr} and the fact our definition of U_{cr} does indeed identify the onset of FEI gives us confidence that our method is robust and reliable. We now apply it to investigate the dependence of FEI on Reynolds number, independent of reduced velocity at a fixed Scruton number.

5. Simulation results and discussion

5.1. Basic parameters of the simulation

Our strategy to uncover the effect of Reynolds number on critical flow velocity is to simulate the flow through moving tube arrays, for a wide range of Reynolds numbers and at a range of flow velocities at which FEI is expected to occur. To separate the effects of (reduced) cross-flow velocity and turbulence, we independently vary cross-flow velocity and Reynolds number at a fixed Scruton number.

As mentioned earlier, in order to avoid interference between lock-in and FEI, the parameters are chosen so that synchronization lock-in does not occur.

As emphasized earlier, simulations are expensive for the moderate and high Reynolds numbers characterizing turbulent flows. It is therefore crucial to choose the key parameters of the problem such that we capture the desired results using a minimum of computation. Our choice of parameters is based on the physics of the problem and the experimental studies reviewed in Section 1.

We consider two cases: in-line and rotated (staggered) square arrays with a pitch-to-diameter ratio $P/D = 1.5$ (see Fig. 1). This is relatively tight spacing typical of the experimental results and industrial installations. The computational periodic until cell has two rows of tubes, $N_T = 2$ (2×2 tubes per periodic domain) since this is the minimal configuration that allows both the in-phase and anti-phase tube oscillations typical of FEI. We have checked that including an additional row, $N_T = 3$, gives similar results for vortex shedding and Strouhal number for the fixed tube case. Considering the time and the available resources, we chose $150 \leq Re_g \leq 9600$ (in-line array) and $210 \leq Re_g \leq 27\,200$ (rotated array) to analyze turbulence intensity and Reynolds number effects on the onset of FEI. We considered a wider range of Reynolds numbers for the rotated array because this configuration is much more sensitive to variations in Reynolds number. This range of Reynolds numbers corresponds well with typical experimental values (when this number is reported). For example, Weaver et al. (1993) considered rotated square arrays with $1392 \leq Re_g \leq 33\,659$.

All parameters are non-dimensionalized with respect to the tube diameter, mean flow velocity and fluid density.

Since our focus is the onset of FEI, using the Blevins experimental results (see Fig. 2) we choose parameters such that the lock-in phenomenon (resonant excitation with vortex shedding) does not occur or interfere with the self-excitation of tubes. Considering all the factors discussed earlier, for each of the simulations we set the Scruton number $Sc = 10$ and the natural frequency $f_N = 1$. In this way, the range of flow velocities where lock-in occurs is fixed and should be sufficiently well-separated from the fluid-elastic vibrations (see Fig. 3). Note that $Sc = 10$ is in the middle range of cases considered in previous experimental investigations, $10^{-1} < Sc < 10^3$. This is because we want the tubes to oscillate easily and are unstable at relatively low flow velocities.

In addition to ensuring that the critical velocity for FEI is well-separated from lock-in and that the tubes are unstable at low flow velocities, the choice of $Sc = 10$ places us just above (for the in-line array) or in (for the rotated array) the multiple stability region for small Scruton numbers predicted by Lever and Weaver's semi-empirical theory (Lever and Weaver, 1986a,b). These multiple stability regions are shown as a sequence of "tongues" in the lower left of Fig. 2(a) and (b). If this theory is accurate, it suggests that the flow could be particularly sensitive to turbulence effects at this Scruton number. Critical flow velocities are calculated as described in Section 3.4 independent of turbulence buffeting level.

Because we use numerical experiments to identify the onset of FEI, and the instability may take a long time to occur, particularly where it is close to instability threshold, the length of the simulation is an important parameter. Generally, a longer simulation time gives better converged statistical results, but available computational resources limit the practical maximum simulation times (especially at the higher Reynolds numbers). We stop the simulations at $t = T_{end}$ once the fluid flow regime is fully developed and the tube responses have converged to statistically steady state RMS values to within a few percent. T_{end} is therefore not a fixed parameter and is determined separately for each simulation.

5.2. Effect of Reynolds number on fluid-elastic instability in an in-line square array

Contour plot 11(a) shows the RMS values of tube vibrations in an in-line array in the transverse flow direction as a function of Re_g and U_r for $Sc = 10$, where the small black circles indicate simulation results. Fig. 11(c) compares critical flow velocities with the dashed lines denoting the mean critical U_{cr} for the experimental results as shown in Fig. 2. It is important to note that the experimental results do not indicate the Reynolds number range in which they are supposed to be valid, but they are definitely turbulent (e.g. $Re_g = O(10^3$–$10^4)$ or greater) and generally higher at smaller Scruton numbers (because of differences in cross-flow fluid).

We performed 42 simulations, covering a considerable range of flow velocities above the lower stability bound and close to the onset of expected FEI, for gap-based Reynolds numbers of 150–9600, spanning both laminar and turbulent flow regimes. The unstable motion is characterized by transverse vibrations (as shown in Fig. 10), with adjacent columns moving exactly anti-phase. There is a very sharp increase in RMS oscillation amplitudes with flow velocity which is consistent with the dynamics of FEI discussed in Section 2.2. The critical flow velocity (white circles) varies somewhat with Reynolds number, but is consistent with the experimental data as shown in Fig. 11(c). This consistency with experimental results further validates our numerical model and choice of model-free two-dimensional direct numerical simulation. Overall, the critical velocity varies relatively little (by about 14%) from its mean value for the range of Reynolds numbers considered.

The fact that the critical velocity is relatively independent of Reynolds number is consistent with the observations of Kevlahan (2011) who found that potential flow calculations give accurate results for the critical velocity for a wide range of phase lags between the cylinder motion and fluid force for the in-line array. We will see in Section 5.3 that, in contrast, the stability of the rotated array decreases strongly with increasing Reynolds number until quite high Reynolds numbers.

Although the critical velocity for the in-line array remains reasonably close to the experimental data for all Reynolds numbers, for $150 < Re_g < 1200$ the tubes are more stable at $Re_g = 600$ than they are at either $Re_g = 300$ or $Re_g = 1200$. In order to better understand this phenomenon, it is helpful to take a closer look at the vorticity dynamics.

At the anomalously stable Reynolds number $Re_g = 600$ Fig. 15 shows the flow has an extremely regular and wavy jet like wake without complete vortex shedding. This particular wavy wake that does not occur at other Reynolds numbers and might be the cause of increased stability at this Reynolds number since the wavelength of the wake appears to precisely match the gap between the tubes. Interestingly, even the unstable velocities at $Re_g = 600$ have lower vibration amplitudes than the neighboring Reynolds numbers. If a precise match between the wake structure and the tube spacing have a stabilizing effect at this Reynolds number, modifying the tube spacing should have strong affect on stability. To check this hypothesis, we performed other simulations keeping the reduced gap velocity, Scruton and Reynolds numbers fixed

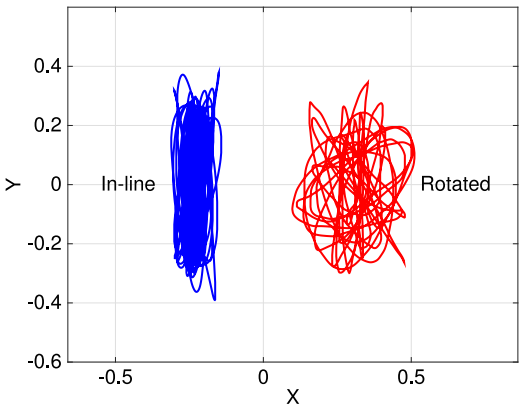

Fig. 10. Typical trajectories of unstable tube oscillations for an in-line array (at $Re_g = 9600$ and $U_r = 12$) and a rotated array (at $Re_g = 6800$ and $U_r = 8.5$). The in-line array has primarily transverse oscillations while the rotated array has whirling oscillations.

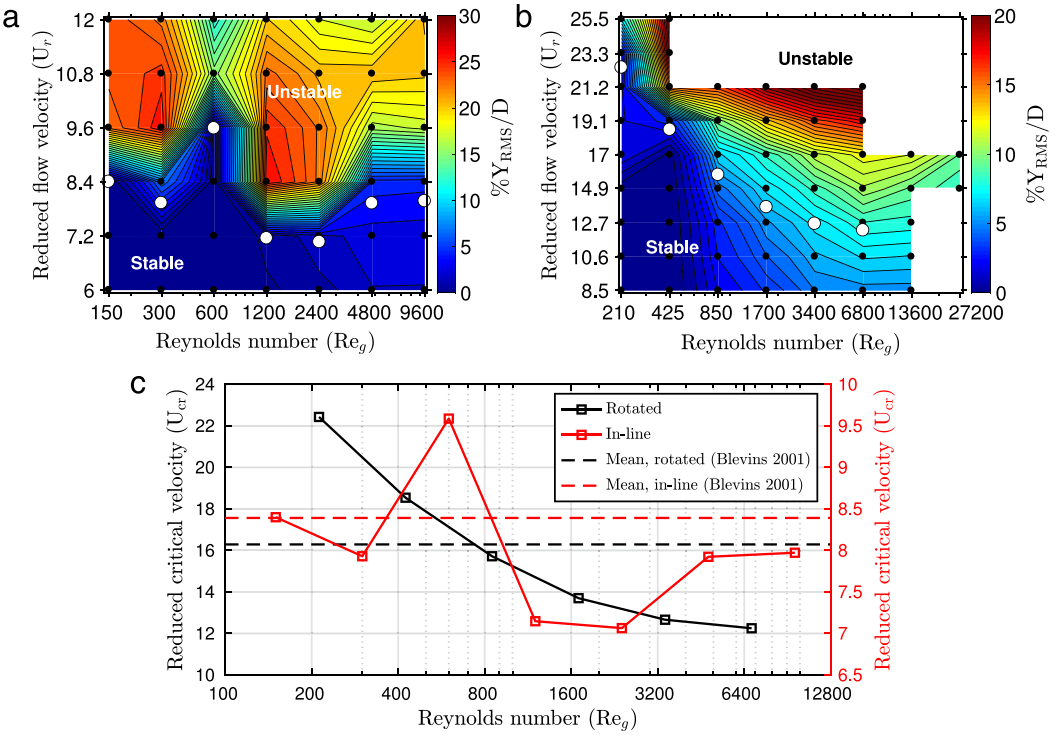

Fig. 11. RMS tube vibration as a function of Reynolds number Re_g and reduced flow velocity U_g in (a) the in-line square array (b) the rotated square array. The white circles correspond to critical flow velocities. In (c) U_{cr} values are compared with the horizontal dashed lines corresponding to the mean values from linear fits to the experimental data shown in Fig. 2. (For interpretation of the references to color in this figure legend, the reader is referred to the web version of this article.)

and varying only the pitch-to-diameter ratio from 1.4 to 2.0 (i.e. varying the gap between the tubes from 0.4 to 1.6). The simulation results confirm that the onset of FEI is very sensitive to the array spacing in the in-line case at this Reynolds number. Even a slightly tighter array ($P/D = 1.4$) is unstable whereas looser packings ($1.5 \leq P/D \leq 2.0$) are stable.

Therefore, we conclude that interaction between gap size and wake geometry can sensitively modify the onset of FEI, at least at low Reynolds numbers in the in-line array.

Interestingly, the results suggest that vibration amplitude does not always grow with U_r and Re_g. The most unstable combination is actually at relatively low velocities and Reynolds numbers $U_r \approx 9$ and $Re_g \approx 1200$. There is another strong peak at $U_r \approx 10.8$ and laminar Reynolds number $Re_g \approx 300$. This non-monotonicity in U_r and Re_g is surprising and we will see it is quite different from the rotated array case.

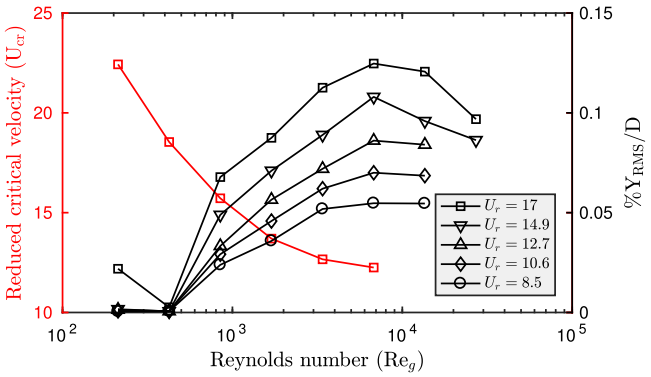

Fig. 12. Critical flow velocity in rotated array (left axis) and tube responses for various flow velocities (right axis). There is a peak in RMS values at $Re_g = 6800$. (For interpretation of the references to color in this figure legend, the reader is referred to the web version of this article.)

Overall, the results show that FEI of the in-line array is relatively insensitive to Re_g and is characterized by a sharp transition between stable and unstable states with increasing U_r. It is interesting to note, however, that for fixed $Sc = 10$ and $U_r \approx 8.4$ the flow may be either stable or unstable depending on Re_g, and that this Reynolds number dependence is *not* monotonic. This complicated dependence of critical reduced velocity on Reynolds number could have contributed to the scatter in the data, where experiments at different Reynolds numbers are plotted together.

5.3. Effect of Reynolds number on fluid-elastic instability in a rotated square array

We now consider the rotated array with the same Scruton number and geometry as the in-line array considered in Section 5.2. We performed 53 simulations for different cross-flow velocities and Reynolds numbers to investigate how the instability threshold changes with U_r and Re_g. As shown in Fig. 10, the unstable motion is qualitatively different from the in-line array and is characterized by whirling motion with adjacent tubes moving independently.

The contour plot 11(b) shows RMS tube response (black circles) in the transverse flow direction as a function of reduced gap velocity U_r and Reynolds number Re_g. The white circles show critical flow velocities. Similar to the in-line array, critical flow velocities are plotted compared to the experimental data for mean U_{cr} in Fig. 11(c).

In contrast to the in-line array, for the rotated array RMS vibration amplitude increases gradually, smoothly and monotonically with both the U_r and Re_g. This smoother growth in tube vibration is likely due to the fact that, unlike the in-line case, the wake of the rotated array is characterized by complete vortex shedding and strong vortex dynamics at all Reynolds numbers (see Fig. 16). There is no abrupt transition to complete vortex shedding and the tube motion and vortex shedding is not synchronized between adjacent row or columns. In addition, even in the stable region, we observe some intermittent random turbulence-induced buffeting with an amplitude increasing gradually with Reynolds number.

The most important new information in the Fig. 11(b), (c) is how critical U_r varies with Re_g in the rotated array. The Reynolds number effect in rotated arrays is much more significant than the in-line case, since the critical U_r decreases steadily by more than 45% as the Reynolds number Re_g increases from 210 to 6800. The critical velocity decreases monotonically with increasing Reynolds number until $Re_g \approx 6800$.

For $Re_g > 6800$, our simulation results are not sufficient to compute U_{cr} since FEI does not appear. However, from the available results it appears that turbulence buffeting decreases for larger Reynolds numbers, $Re_g = 6800$ to $Re_g = 27\,200$, since the level of RMS fluctuations is lower overall (see Fig. 12). This is in contrast to the simulation results for lower Reynolds numbers up to $Re_g = 6800$ where turbulence buffeting increases with Reynolds number while U_{cr} drops considerably. We tentatively suggest that U_{cr} may increase (stabilizing effect) at $Re_g > 6800$ since the RMS values are lower in the turbulence buffeting region.

These results are interesting because we have shown that increasing Reynolds number and reduced velocity have qualitatively different effect on FEI for in-line and rotated arrays. Rotated arrays appear to be more sensitive to changes in Reynolds numbers, at least for $Re_g < 6800$. However, the dependence on both Reynolds number and reduced velocity is smooth and monotonic. Increasing U_r or Re_g always leads to higher RMS tube vibration, probably due to increased turbulence buffeting. This suggests that the FEI of rotated arrays at high Reynolds numbers should be easier to predict than that of in-line arrays.

Overall as Fig. 11(c) suggests, critical flow velocity is much larger than the mean U_{cr} based on experimental data at low Reynolds number and is less than the mean value for $Re_g > 800$. This finding helps explain the large uncertainty in experimental studies. It is also appropriate at this point to recall that all the previous experimental data, as well as theories and design guidelines, have ignored the effect of Reynolds number on FEI or have reported it as an unclear factor. The fact that in-line and rotated arrays respond differently to increasing Reynolds numbers could have led to this uncertainty.

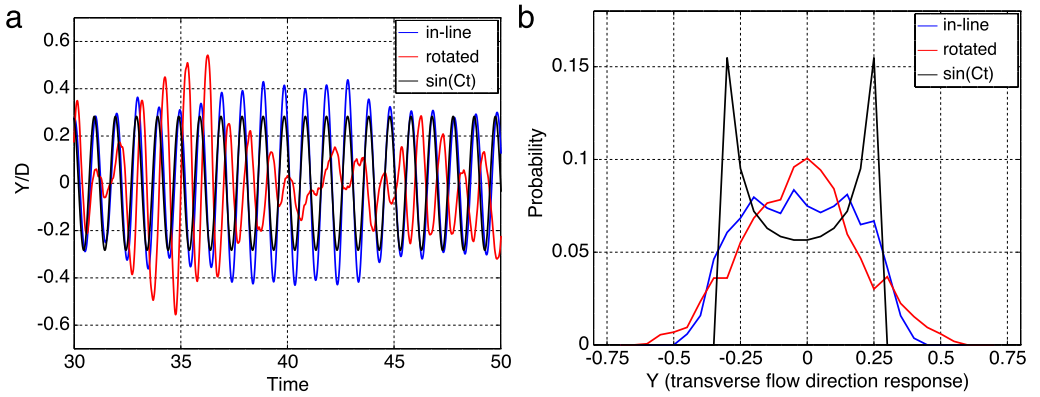

Fig. 13. (a) Tube response in an unstable region for an in-line and a rotated array compared to a sine function with the same RMS values. (b) The corresponding histogram of tube positions for the same tube arrays, compared to sine function.

5.4. Tube vibration dynamics

As noted above, Fig. 11(a), (b) show that the onset of FEI in the in-line array is sharper with respect to a small increase in the U_r than in the rotated array. The tube vibration responses in these two configurations are also qualitatively different. Fig. 13 shows typical transverse tube displacements and histograms of tube displacement for in-line and rotated arrays with the same unstable Y_{rms}/D value of 20%. The responses in the in-line array is closer to a sine wave, in which the displacement amplitude change slightly over time. On the other hand, the displacement amplitudes of the tubes in the rotated array vary significantly and rapidly from zero to a relatively high values. This means that rotated arrays have higher *maximum* amplitudes than in-line arrays for the same Y_{rms}/D values and RMS values are less representative of maximum tube vibration for rotated arrays than for in-line arrays. In other words, rotated arrays are characterized by more extreme oscillation events than the more regular vibrations of the in-line arrays.

6. Discussion: the role of turbulence in FEI

In order to better understand the FEI results of the previous section we consider the equivalent static case of four fixed tubes per periodic domain. The static case is important for understanding the onset of instability since it is the unperturbed case that becomes unstable due to the interaction of fluid forces and the mechanical properties of the system. In Section 2.1 we noted that increasing Reynolds number could affect tube stability in three ways: increasing turbulence damping (stabilizing), higher fluctuating fluid forces (de-stabilizing) and broadening the frequency of vortex shedding (de-stabilizing). We will consider each of these effects in turn for the static array.

6.1. Turbulent damping

For small displacements the fluid damping for transverse oscillations may be approximated as (Kevlahan, 2011), $\frac{1}{2}UDC_D$, which is proportional to the drag force C_D for a given mean flow velocity U and tube diameter D. The level of turbulence modifies C_D compared to its laminar value, and for some turbulent flows C_D may also vary with Reynolds number. Fig. 14 shows that the RMS drag force is essentially independent of Reynolds number for the rotated array (it varies by less than 6% from its mean value of 1.57), and increases by just 12% as Reynolds number increases eightfold from 400 to 3200 in the in-line array. Thus, it is unlikely that increased stability due to increasing turbulence damping is a significant effect of increasing Reynolds numbers for the rotated arrays. This is consistent with the fact that tube vibration was found to increase monotonically with Reynolds number.

In contrast, for the in-line arrays RMS C_D varies by increases by about 25% from its low Reynolds value of 0.52 to its higher Reynolds number value of 0.71 as Re_g increases from 2500 to 5000. This jump in drag appears to coincide approximately with the transition to more turbulent flow (compare Fig. 15(d) and (e)). This is not an extremely strong effect, but does suggest that, in contrast to the rotated array, increasing Reynolds number does lead to more damping and hence lower tube vibration. This is consistent with the results in Fig. 11 which show lower tube amplitudes at higher Reynolds numbers.

6.2. Increasing fluid forces

We have seen that drag force is approximately independent of Reynolds number for rotated array, but jumps significantly for the in-line array as the flow becomes fully turbulent. In contrast, Fig. 14 shows that both arrays feel a large increase in RMS lift force with increasing Reynolds number. The RMS lift grows steadily with increasing Reynolds number until the

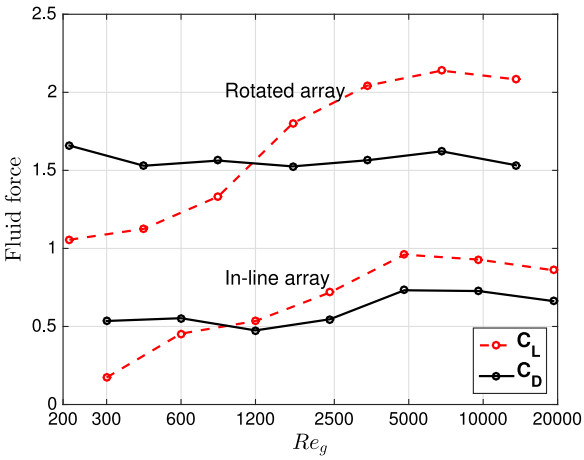

Fig. 14. Variation in RMS lift C_L and drag C_D with Reynolds number Re_g for the two static arrays at fixed $U_r = 3$ (based on U_∞). Note that RMS drag is relatively insensitive to Reynolds number while RMS lift increases dramatically with increasing Reynolds number before stabilizing for $Re_g > 5000$.

flows are fully turbulent, at $Re_g \approx 5000$, where they stabilize near $C_L = 2$ for the rotated array and $C_L = 1$ for the in-line array.

Even though the lift forces are twice as large for the rotated array, the typical critical U_r for the rotated array is about twice that of the in-line array. This shows that the rotated array is far more stable than the in-line array, probably because the whirling tube motions are largely de-synchronized between rows and columns.

Note, however, that for the in-line array the growth in RMS C_L (de-stabilizing) is mirrored by the growth in RMS C_D (stabilizing) which suggests the two effects might compensate each other. In contrast, in the rotated array the growth in RMS C_L is not compensated by a corresponding increase in turbulence damping. These results are again consistent with the FEI results presented in Fig. 11 which show a stronger dependence on Reynolds number for the rotated array until relatively high Reynolds numbers, $Re_g > 6800$.

6.3. Vortex shedding

We now consider the third possible effect of Reynolds number on FEI: changes in the vortex shedding frequency. Recall that we have deliberately chosen the simulation parameters so that we are well outside of the lock-in (resonant vortex shedding) regime for the peak Strouhal frequency. However, it is possible that increasing turbulence could broaden the peak Strouhal frequency, possibly exciting unstable FEI modes.

Figs. 15 and 16 show representative vorticity fields for the in-line and rotated arrays at a range of turbulent and non-turbulent Reynolds numbers. The two arrays have very different wake structures before the flows become full turbulent at $Re_g > 2400$. At the lowest Reynolds numbers $Re_g = 300$ and 600 the in-line flow has a wavy jet-like wake with incomplete vortex shedding. At intermediate Reynolds numbers $Re_g = 1200$ and 2400 vortex shedding is complete, but vortex shedding is still largely synchronized between all tubes. In contrast, Fig. 16 shows that the rotated array is characterized by complete vortex shedding even at the lowest Reynolds numbers $Re_g = 210$ and 425. Vortex shedding from adjacent tubes also de-synchronizes at a much lower Reynolds number, $Re_g = 850$. However, once the turbulence is fully developed (Figs. 15 and 16 (e) and (f)) the vortex structure is qualitatively similar for both arrays (although the rotated array has much higher vorticity levels). These qualitative vortex shedding characteristics are consistent with the FEI results which show the in-line array is more unstable and the critical U_r in the rotated array has a monotonic dependence on Reynolds number. They also agree with the observation that critical U_r stabilizes at sufficiently high Reynolds numbers.

Fig. 17 shows the frequency spectrum of the non-dimensional lift force (C_L) for one of the tubes in the in-line and rotated arrays at various Reynolds numbers. These plots illustrate some important qualitative differences between the two arrays and the effects of increasing Reynolds number on VIV.

At $Re_\infty \leq 200$ there is a single well-defined dominant vortex shedding frequency in the rotated array and the lift force amplitude is also large. This is because flow is laminar and structured. There is also a dominant vortex shedding frequency for the in-line array, but it is relatively small because vortex shedding is incomplete and the flow is jet-like.

For larger Reynolds numbers, $Re_\infty \geq 400$, the flow gradually becomes turbulent and the lift force frequency bandwidth increases considerably. The higher the Reynolds number, the wider the frequency spectrum and the stronger the vortex shedding. The effect of this increased range of excited vortex shedding frequencies on FEI is unclear.

The turbulence intensity, the ratio of RMS velocity to mean velocity, is very high for tube arrays compared to a homogeneous isotropic turbulent flow at a similar Reynolds number. The tube arrays have typical turbulence intensities of 80%–150% due to the strong interactions between adjacent vortical wakes compared to 5%–15% for homogeneous isotropic

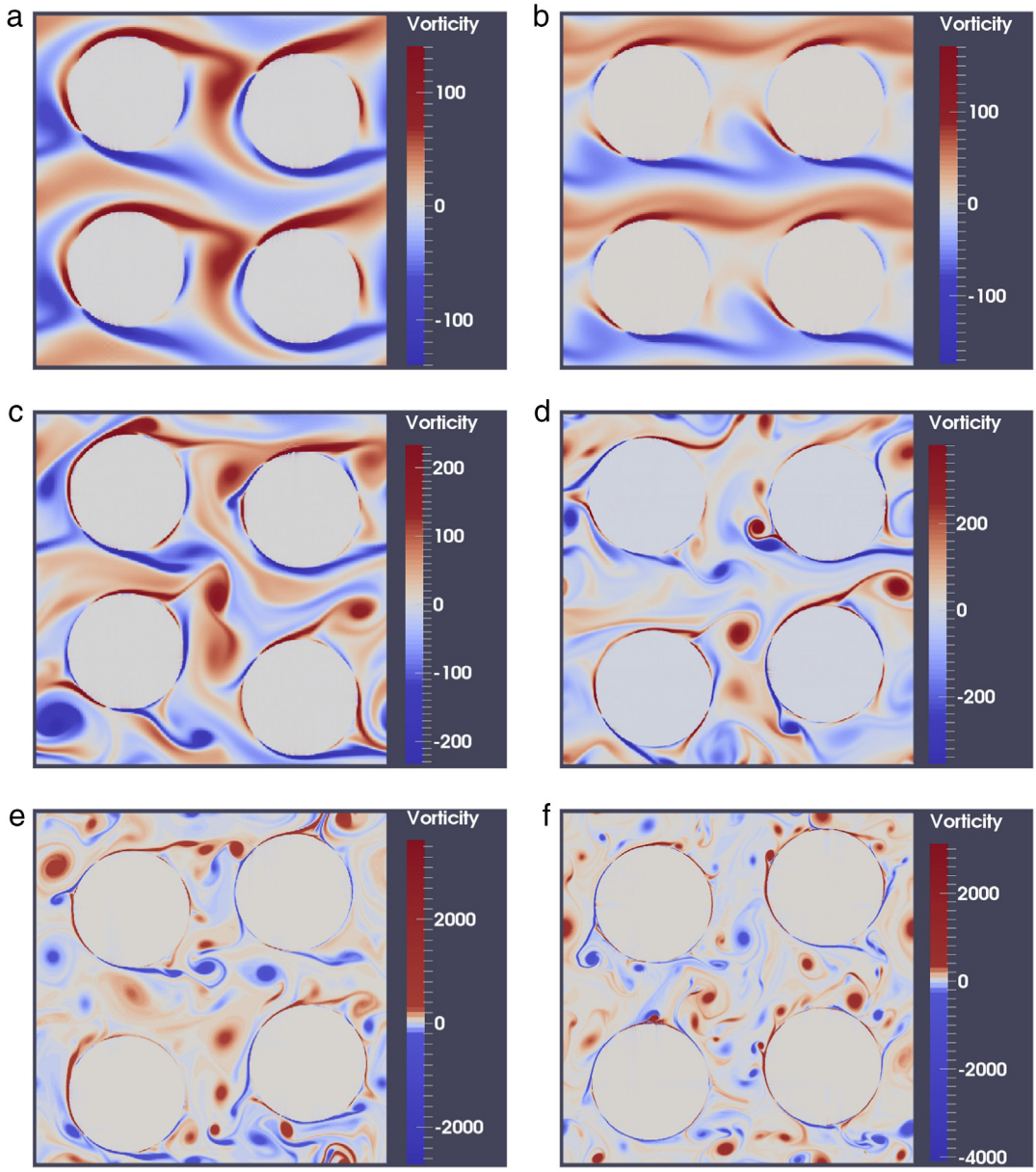

Fig. 15. Vorticity fields at (a) $Re_g = 300$, (b) $Re_g = 600$, (c) $Re_g = 1200$, (d) $Re_g = 2400$, (e) $Re_g = 4800$, (f) $Re_g = 9600$, for moving in-line tube array subjected to cross-flow $U_r = 9.0$.

turbulence. This means that random turbulence buffeting should be a strong effect in the rotated array, where vortex shedding is largely uncorrelated between nearby tubes.

In summary, flow through the tube array is characterized by two distinct flow regimes, one is structured and laminar ($Re_g \leq 600$) and the other is unstructured and turbulent ($Re_g \geq 1200$). The laminar regime is characterized by a single dominant vortex shedding frequency while the turbulent regime is characterized by multiple vortex shedding frequencies that could more easily excite tube instabilities, as discussed in Section 2.1. These multiple shedding frequencies could combine with the higher lift forces noted earlier to increase tube vibrations in the rotated array where higher lift forces are not compensated by increased turbulence damping.

7. Conclusions

The goal of this paper is to better understand the role of Reynolds number and turbulence in the onset of fluid elastic instability (FEI) in tube arrays. The effect of Reynolds number on FEI has been controversial, with some experimental studies

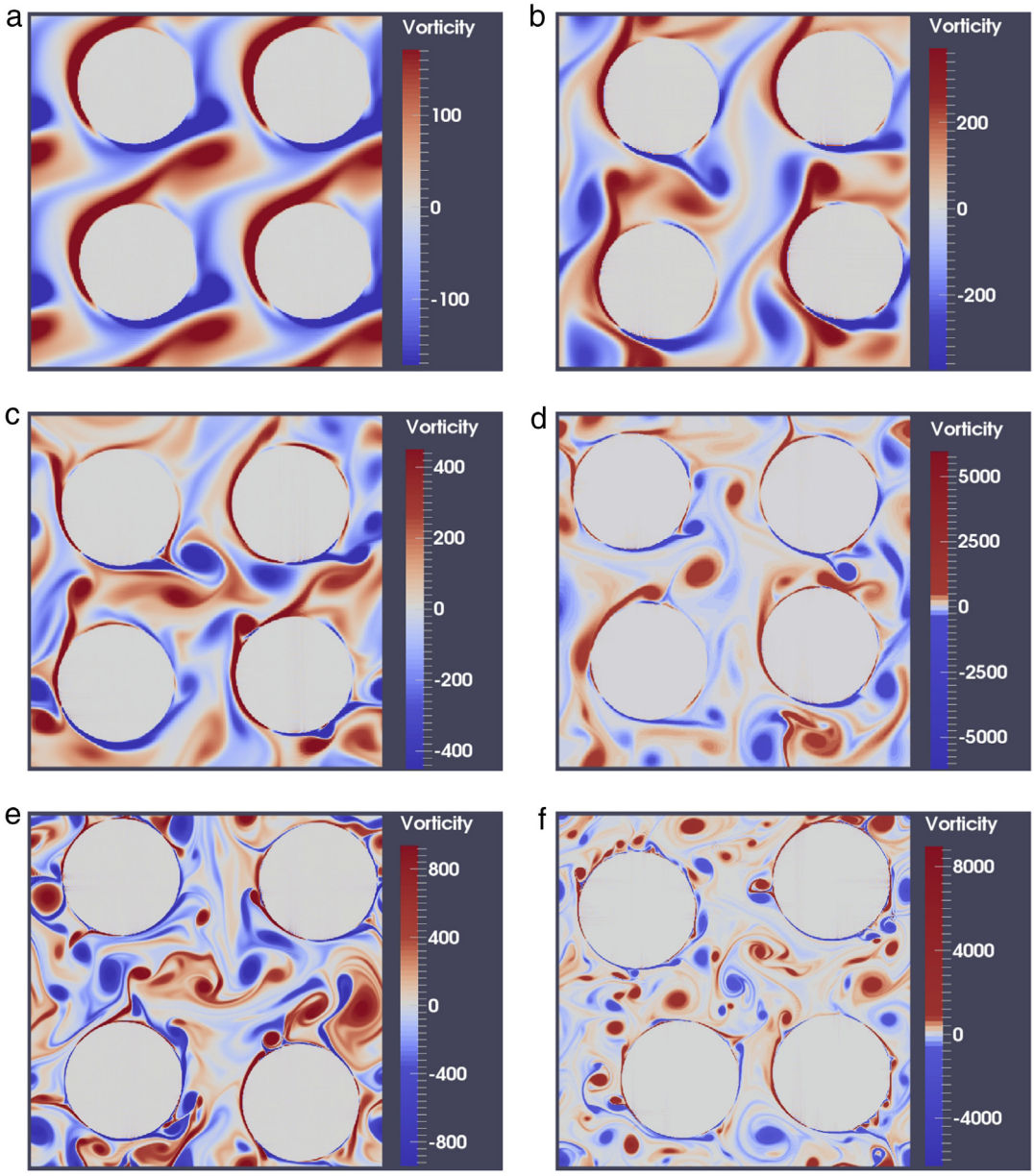

Fig. 16. Vorticity fields at (a) $Re_g = 210$, (b) $Re_g = 425$, (c) $Re_g = 850$, (d) $Re_g = 1700$, (e) $Re_g = 3400$, (f) $Re_g = 6800$, for moving rotated tube array subjected to cross-flow $U_r = 21.2$.

claiming that increased Reynolds number is stabilizing and others that it is de-stabilizing. Often, experimental results do not even report the Reynolds number, which may account for the large scatter in the data. This is the first comprehensive attempt to analyze the actual role of turbulence and Reynolds number in FEI independently of reduced velocity at a fixed Scruton number.

To investigate FEI in tube arrays we have developed a parallelized two-dimensional Fourier pseudo-spectral direct numerical simulation (DNS) method. This approach uses a volume penalization method to account for the moving cylinders and builds on earlier work (Kevlahan, 2011). The two-dimensional model was validated against experimental data for Strouhal number and for the dependence of FEI on reduced velocity U_r and Scruton number Sc. This validation confirmed the usefulness of the two-dimensional DNS approach.

We considered in-line and rotated square arrays of circular cylinders with a pitch-to-diameter ratio of 1.5, configurations often used in experiments.

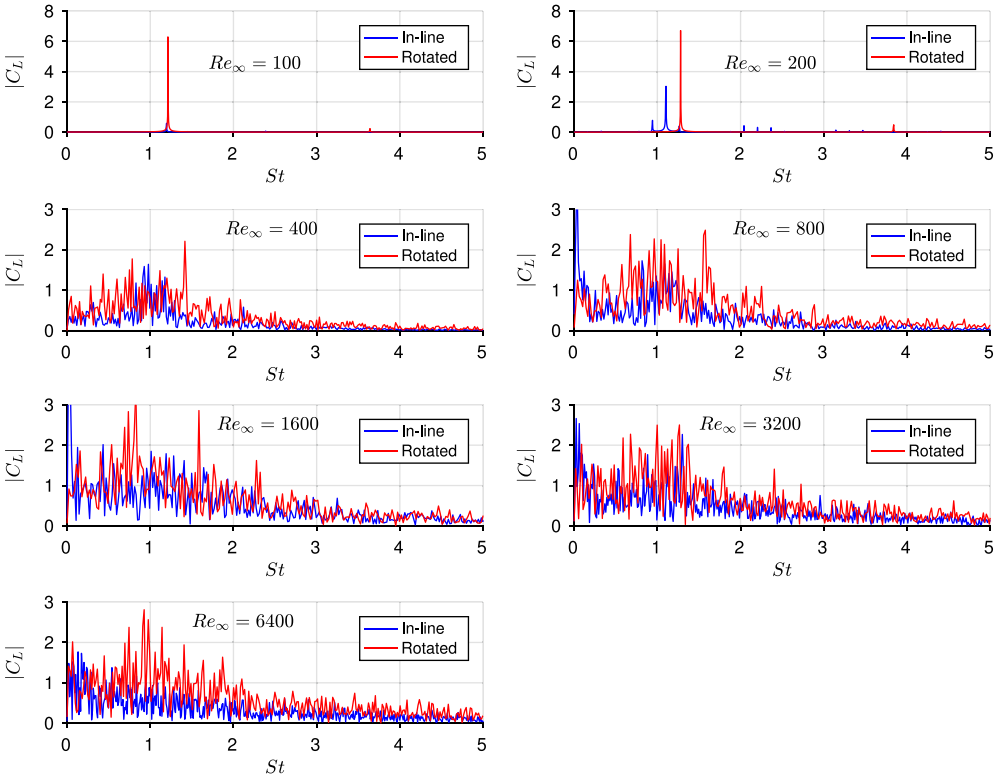

Fig. 17. Lift force (C_L) frequency spectrum at a variety of Reynolds numbers for fixed in-line and rotated arrays. The Strouhal and Reynolds numbers are defined using the upstream velocity $U_\infty = 3$. $U_r = 9$ for the in-line array and $U_r = 6.36$ for the rotated array, based on the gap velocity. Note that the natural frequency of the tubes ($St = 1/3$) is excited for $Re_\infty \geq 400$ (corresponding to $Re_g \geq 1200$ for the in-line array and $Re_g \geq 850$ for the rotated array).

The two array configurations respond very differently to increasing Re_g due to differences in vortex dynamics. The critical U_r for FEI in the in-line array is relatively insensitive to Re_g over the range $150 \leq Re_g \leq 9600$, but with a non-monotonic dependence of critical U_r on Re_g. Surprisingly, we find the largest tube vibration amplitudes at relatively low U_r and Re_g: $U_r \approx 9$ and $Re_g \approx 1200$. The non-monotonic response of in-line tube arrays to increases in Reynolds numbers might explain the claims of Southworth and Zdravkovich (1975) and Soper (1982) that turbulence has a stabilizing effect for in-line arrays.

In contrast, increasing Re_g leads to considerably decreased critical flow velocity for the rotated array for $210 \leq Re_g \leq 6800$. Therefore, Reynolds number in this range always has a destabilizing effect on the rotated tube array. Moreover, one can perhaps expect the stability threshold to increase at $Re > 6800$ since once the flow becomes fully turbulent at $Re > 6800$, we found that turbulence buffeting becomes weaker with increasing Reynolds number. In addition, the change dU_{cr}/dRe_g is close to zero at $Re_g = 6800$ which suggest this Reynolds number might be a turning point for U_{cr}.

The trajectories of unstable tube motion are qualitatively different for the two arrays. Tubes in the in-line array move transversely to the mean flow with adjacent columns moving exactly anti-phase. Tubes in the rotated array move in a whirling (roughly circular) motion with little synchronization between adjacent tubes. These motions are related to the different vortex wake structures in the two arrays, with the in-line array having a more regular jet-like wake with incomplete or weaker vortex shedding (at low and moderate Re_g) while the rotated array is characterized by strong alternating vortex shedding. This results in distinct statistics for tube motion, with the in-line array having regular sinusoidal tube motion (well-characterized by RMS tube displacement) while the rotated array has much more frequent extreme tube displacements.

We attempted to understand these results by looking at three ways increasing Re_g might affect FEI: more turbulence damping (stabilizing), higher fluctuating fluid forces (de-stabilizing) and broadening the frequency of vortex shedding (de-stabilizing). We found that turbulence damping is essentially independent of Re_g for the rotated array, but jumps by about 25% for the in-line array when the flow transition to turbulence. On the other hand, RMS lift forces increase dramatically with increasing Re_g in both arrays before finally stabilizing when the flows are fully turbulent. Since increased fluid damping compensates for increased lift in the in-line array, these observations could explain the relative insensitivity of FEI in this array to increasing Re_g. Finally, we found that the spectrum of vortex shedding frequencies broadens dramatically as the flow becomes turbulent. For $Re_\infty \geq 400$ the natural frequency of the tubes is excited and the broad range of higher excited frequencies could produce the phase lag between tube motion and lift force necessary for FEI. This means that increasing Re_g raises the probability of triggering unstable FEI modes until Re_g is high enough that all potential unstable modes have been excited.

The results presented here have helped untangle the effects of reduced velocity and turbulence in FEI of tube arrays. They have also demonstrated the practical usefulness of two-dimensional DNS for simulating these flows at turbulent Reynolds numbers.

Acknowledgments

NKRK acknowledges the support of an NSERC Discovery Grant. We thank Compute Canada and SHARCnet for providing computational resources for the numerical simulation results reported in the paper.

References

Angot, P., Bruneau, C.-H., Fabrie, P., 1999. A penalization method to take into account obstacles in incompressible viscous flows. Numer. Math. 81 (4), 497–520.
ASME, , 1995. ASME Boiler and Pressure Vessel Code. ASME, Section III Rules for Construction of Nuclear Power Plant Components Division 1 - Appendices. pp. 370–397.
Blevins, R., 1984. Review of sound induced by vortex shedding from cylinders. J. Sound Vib. 92 (4), 455–470.
Blevins, R., 2001. Flow-Induced Vibration, second ed. Krieger Publishing Company.
Carbou, G., Fabrie, P., et al., 2003. Boundary layer for a penalization method for viscous incompressible flow. Adv. Differential Equations 8 (12), 1453–1480.
Chen, Y., 1968. Flow-induced vibration and noise in tube-bank heat exchangers due to von Karman streets. Trans. ASME, J. Manuf. Sci. Eng. 90 (1), 134–146.
Chen, S., 1978. Crossflow-induced vibrations of heat exchanger tube banks. Nucl. Eng. Des. 47 (1), 67–86.
Chen, S.-S., 1987. Flow-Induced Vibration of Circular Cylindrical Structures. Hemisphere Publishing, New York, NY.
Chen, S.S., Jendrzejczyk, J.A., 1981. Experiments on fluid elastic instability in tube banks subjected to liquid cross flow. J. Sound Vib. 78 (3), 355–381.
Chung, H.J., Chu, I.-C., 2006. Fluid-elastic instability of rotated square tube array in an air-water two-phase crossflow. Nucl. Eng. Technol. 38 (1), 69–80.
Connors, H., 1970. Fluidelastic vibration of tube arrays excited by cross flow. In: Proc. ASME Winter Annual Meet., 1970.
Fitzhugh, J., 1973. Flow-Induced Vibration in Heat Exchangers. Tech. rep., Oxford University, RS57 (AERE P7238).
Franklin, R., Soper, B., 1977. An investigation of fluidelastic instabilities in tube banks subjected to fluid cross-flow. In: 4th International Conference on Structural Mechanics in Reactor Technology, SMiRT. p. F6/7.
Kevlahan, N.K.-R., 2007. Three-dimensional Floquet stability analysis of the wake in cylinder arrays. J. Fluid Mech. 592, 79–88.
Kevlahan, N.K.-R., 2011. The role of vortex wake dynamics in the flow-induced vibration of tube arrays. J. Fluids Struct. 27, 829–837. http://dx.doi.org/10.1016/j.jfluidstructs.2011.03.023.
Kevlahan, N.-R., Ghidaglia, J.-M., 2001. Computation of turbulent flow past an array of cylinders using a spectral method with Brinkman penalization. Eur. J. Mech. B Fluids 20 (3), 333–350.
Kevlahan, N.-R., Wadsley, J., 2005. Suppression of three-dimensional flow instabilities in tube bundles. J. Fluids Struct. 20 (4), 611–620.
Lever, J., Weaver, D., 1982. A theoretical model for fluid-elastic instability in heat exchanger tube bundles. Trans. ASME, J. Press. Vessel Technol. 104 (3), 147–158.
Lever, J., Weaver, D., 1986a. On the stability of heat exchanger tube bundles, Part I: modified theoretical model. J. Sound Vib. 107 (3), 375–392.
Lever, J., Weaver, D., 1986b. On the stability of heat exchanger tube bundles, Part II: numerical results and comparison with experiments. J. Sound Vib. 107 (3), 393–410.
MacDonald, P., Shah, V., Ward, L., Ellison, P., 1996. Steam Generator Tube Failures. Tech. Rep., Nuclear Regulatory Commission, Washington, DC (United States). Div. of Safety Programs.
Meriam, J., Kraige, L., 2013. Engineering Mechanics: Dynamics, seventh ed. John Wiley & Sons.
Mewes, D., Stockmeier, D., 1991. Fluid viscosity effects on flow induced vibrations of tube bundles in cross-flow. In: Proceedings of 5th International Conference on Flow Induced Vibrations, Brighton. pp. 231–242.
Nakamura, T., Kaneko, S., Inada, F., Kato, M., Ishihara, K., Nishihara, T., Mureithi, N., 2013. Flow-Induced Vibrations: Classifications and Lessons from Practical Experiences. Butterworth-Heinemann.
Païdoussis, M.P., Price, S.J., de Langre, E., 2010. Fluid-Structure Interactions: Cross-Flow-Induced Instabilities, first ed. Cambridge University Press.
Price, S., Païdoussis, M., 1984. An improved mathematical model for the stability of cylinder rows subject to cross-flow. J. Sound Vib. 97 (4), 615–640.
Price, S., Païdoussis, M., Mark, B., et al., 1995. Flow visualization of the interstitial cross-flow through parallel triangular and rotated square arrays of cylinders. J. Sound Vib. 181 (1), 85–98.
Roberts, B.W., 1966. Low Frequency, Aeroelastic Vibrations in a Cascade of circular Cylinders. In: Mechanical Engineering Science Monograph, vol. 4.
Sarpkaya, T., 2004. A critical review of the intrinsic nature of vortex-induced vibrations. J. Fluids Struct. 19 (4), 389–447.
Shellard, H., 1967. Collapse of cooling towers in a gale, Ferrybridge, 1 November 1965. Weather 22 (6), 232–240.
Shinde, V., 2014. Fluidelastic Instability in Heat Exchanger Tube Arrays and a Galerkin-Free Model Reduction of Multiphysics Systems. (Ph.D. thesis), Université Paris Saclay.
Shinde, V., Marcel, T., Hoarau, Y., Deloze, T., Harran, G., Baj, F., Cardolaccia, J., Magnaud, J., Longatte, E., Braza, M., 2015. Numerical simulation of the fluid–structure interaction in a tube array under cross flow at moderate and high Reynolds number. J. Fluids Struct. 47, 99–113.
Soper, B., 1982. The effect of grid generated turbulence on the fluidelastic instability of tube bundle in cross flow. In: Taborek, J., Hewitt, G., Afgan, N. (Eds.), Heat Exchangers: Theory and Practice. International Center for Heat and Mass Transfer, pp. 325–337.
Soper, B., 1983. The effect of tube layout on the fluid elastic instability of tube bundles in cross flow. ASME J. Heat Transfer 105 (4), 744–750.
Southworth, P., Zdravkovich, M., 1975. Effect of grid-turbulence on the fluid-elastic vibrations of in-line tube banks in cross flow. J. Sound Vib. 39 (4), 461–469.
Spiteri, R., Ruuth, S., 2002. A new class of optimal high-order strong-stability-preserving time discretization methods. SIAM J. Numer. Anal. 40 (2), 469–491.
Trefethen, L.N., 2000. Spectral Methods in MATLAB. SIAM.
Weaver, D., Lian, H., Huang, X., 1993. Vortex shedding in rotated square arrays. J. Fluids Struct. 7, 107–121.

Further reading

Paidoussis, M., Price, S., 1988. The mechanisms underlying flow-induced instabilities of cylinder arrays in cross-flow. J. Fluid Mech. 187, 45–59.